Rejuvenation-Responsive and Senolytic-Sensitive Muscle Stem Cells Unveiled by CD200 and CD63 in Geriatric Muscle

Ye Lynne Kim[1†], Young-Woo Jo[1†], Takwon Yoo[1†], Kyusang Yoo[1], Ji-Hoon Kim[2], Myungsun Park[3], In-Wook Song[1], Hyun Kim[1], Yea-Eun Kim[1], Sang-Hyeon Hann[1], Jong-Eun Park[3], Daehyun Baek[1], and Young-Yun Kong[1*].

[1]School of Biological Sciences, Seoul National University, 08826, Seoul, Korea.

[2]Molecular Recognition Research Center, Korea Institute of Science and Technology, Seoul, Republic of Korea.

[3]Graduate School of Medical Science and Engineering, KAIST, Daejeon, Republic of Korea.

[†] These authors contributed equally to this work.

[*] Corresponding author. Email: ykong@snu.ac.kr, Telephone: +82) 02-880-2638, FAX: +82) 02-872-1993

Author contributions:

Conceptualization, Y.L.K., Y.-W.J. and Y.-Y.K.; Data acquisition: Y.-W.J., Y.L.K., T.Y., J.-H.K. Y.-E.K., and S.-H.H.; Data analysis: Y.-W.J., Y.L.K., T.Y., and K.Y.; Technical support: T.Y., M.P., I.-W.S. J.-E.P., and D.B.; Writing: Y.L.K., Y.-W.J., T.Y., and Y.-Y.K.; Supervision: J.-E.P., D.B., Y.-Y.K.

Competing interests: Authors declare that they have no competing interests.

Abstract

Muscle stem cells (MuSCs) are parenchymal cells in skeletal muscle regeneration and maintenance. With aging, MuSCs experience a decline in their regenerative function and reduction in their number. However, recent evidence points to substantial heterogeneity within the aged MuSC population, raising questions about the underlying mechanisms of age-associated dysfunction. Here, we used Pax7^{CreERT2};Rosa^{YFP} mice (MuSC^{YFP}) to label Pax7-expressing MuSCs and chronologically traced MuSCs until geriatric age. Genetic labeling and chronological tracing revealed that the number of YFP^{+} MuSC remained comparable between young, middle and geriatric ages. At geriatric age, YFP^{+} MuSCs exhibited reduced expression of traditional MuSC markers such as VCAM1 and PAX7. A previously unrecognized subpopulation emerged, characterized by loss of VCAM1 and low or absent PAX7. Despite their altered marker profile, these cells retained transcriptional signatures of quiescence and myogenic potential, but displayed significantly reduced proliferative and regenerative capacities. They displayed gene expression patterns indicative of senescence-like state and were selectively ablated by senolytic treatment. DHT restored regenerative function in aged mice and re-induced VCAM1 expression in YFP^{+}/Pax7$^{-/low}$/VCAM1^{-} cells, indicating responsiveness to rejuvenation. Based on their emergence with aging, functional impairment and responsiveness to rejuvenation, we termed this population GERI-MuSCs (Geriatric Emerging Rejuvenation-responsive and Impaired MuSCs). CD63 and CD200 were identified as novel surface markers that together with VCAM1, reliably detect GERI-MuSCs as well as classical Pax7^{+}/VCAM1^{High} MuSCs, providing a tool for comprehensive isolation of MuSCs from aged wild-type mice. Together, our findings provide a refined framework for studying MuSC aging and offer new tools for isolating functionally distinct MuSC subsets from aged skeletal muscle.

Introduction

Skeletal muscle regeneration is orchestrated primarily by tissue resident stem cells, known as muscle stem cells (MuSCs) or satellite cells(Mauro, 1961). MuSCs reside beneath the basal lamina of myofibers in a quiescent state under homeostatic condition but become rapidly activated upon injury to proliferate, differentiate, and fuse into regenerating myofibers(Evano and Tajbakhsh, 2018). While the regenerative function of MuSCs is well maintained in youth, a decline in their number and regenerative competence is observed in aging, leading to impaired muscle repair and tissue maintenance(Blau et al., 2015).

The age-related decline in MuSC function arises from a combination of extrinsic and intrinsic factors. Extrinsic factors include the increased pro-inflammatory cytokines(Degens, 2007), extracellular matrix remodeling(Schuler et al., 2021) and altered mechanical properties of the niche microenvironment(Chakkalakal et al., 2012). MuSC intrinsic factors include disrupted metabolic homeostasis(Pala et al., 2018), loss of proteostasis(Kim et al., 2021b), altered epigenetic regulation(Hernando-Herraez et al., 2019), mitochondrial dysfunction(Rygiel et al., 2016) and aberrant activation of signaling pathways, including p38 MAPK(Bernet et al., 2014), JAK/STAT(Price et al., 2014) and mTORC1(Tang et al., 2019). As a result, aged MuSCs show reduced colony-forming capacity, failure to maintain quiescence and loss of self-renewal potential causing a significant decline in the MuSC pool. This reduction in the resident stem cell population directly undermines the muscle's capacity for effective repair(Blau et al., 2015, Day et al., 2010). Although functional and molecular differences between young and aged MuSCs have been extensively documented, the timing and trajectory by which these alterations arise remain unclear. This study was therefore designed to delineate the transition that occurs between middle-aged and

70 geriatric MuSCs, rather than to re-characterize differences that are already well established
71 between young and aged muscles.
72
73 Efforts to reverse MuSC dysfunction have explored both systemic and cell-intrinsic interventions.
74 Circulating factors identified in parabiosis experiments(Conboy et al., 2005), as well as
75 supplementation with molecules such as NAD^+(Zhang et al., 2016) and oxytocin(Elabd et al.,
76 2014), have shown potential in restoring regenerative capacity. Pharmacological modulation of
77 signaling pathways, such as inhibition of JAK/STAT(Price et al., 2014), p38 MAPK(Bernet et al.,
78 2014), mTORC1, TGF-β or Wnt signaling(Carlson et al., 2009), has led to improved regeneration
79 in aged muscle. However, variation in the age of experimental animals complicates the
80 interpretation of these findings. Many rejuvenation studies define 'aged' mice as 18 to 24 months
81 old. This range encompasses a period of heterogeneous functional decline, during which a
82 substantial fraction of MuSCs may still retain regenerative capacity. Therefore, since it is unclear
83 whether these models fully represent a truly geriatric state, questions remain as to whether these
84 interventions directly restore dysfunctional MuSCs, selectively expand a subset of aged MuSCs
85 that retain partial functionality, or delay or prevent the aging of MuSCs that have not yet undergone
86 substantial aging. To address this uncertainty, we chronologically traced the fate of Pax7-
87 expressing MuSCs in geriatric mice using a genetic labeling system. This allowed us to evaluate
88 the composition, functionality, and responsiveness of aged MuSC subsets.
89
90 In addition to interventions aimed at reversing MuSC dysfunction, an alternative strategy to restore
91 regenerative competence involves targeting senescent cells. Senescent cells accumulate in aged
92 muscle and are thought to impair regeneration through secretion of pro-inflammatory and matrix-

93 remodeling factors, collectively known as the senescence-associated secretory phenotype (SASP)
94 (Saito and Chikenji, 2021). Senolytic agents, such as dasatinib and quercetin, which selectively
95 eliminate senescent cells have been shown to improve tissue homeostasis and extend muscle
96 healthspan in preclinical models(Xu et al., 2018). However, although senescence is broadly
97 defined as a state of irreversible cell cycle arrest accompanied by transcriptional reprogramming,
98 how this process manifests in quiescent adult stem cells *in vivo* remains incompletely understood.
99 This uncertainty raises concerns regarding the use of senolytics, as such treatment may
100 inadvertently eliminate MuSC subsets that retain latent regenerative potential. A better
101 understanding of how senescence-like features emerge within the aged MuSC pool is therefore
102 critical for evaluating the risks and benefits of senolytic treatment in aging muscle.
103
104 In this study, our findings reveal an age-dependent accumulation of a previously unrecognized
105 population of MuSCs, which we termed GERI-MuSCs (Geriatric Emerging Regeneration-capable
106 and Impaired MuSCs). GERI-MuSCs are characterized by low expression of traditional marker
107 genes, impaired yet retained functionality, susceptibility to senolytic deletion, and responsiveness
108 to DHT rejuvenation. Moreover, CD63 and CD200 can be reliable markers that can be used with
109 VCAM1 to detect previously hard-to-detect MuSCs. This combinatorial strategy provides a
110 framework for future isolation and therapeutic targeting of GERI-MuSCs. Together, our results
111 refine the understanding of in vivo MuSC aging and highlight the importance of studying stem cell
112 subsets that are functionally impaired yet not irreversibly senescent.
113
114 **Results**
115 *Genetic labeling of Pax7^{+} cells reveal marker-deficient MuSCs in aged muscle*

116 *Paired box protein 7* (*Pax7*) is a transcription factor widely recognized as a defining marker of
117 MuSCs (Seale et al., 2000). To investigate how aging alters the identity of MuSCs, we used
118 *Pax7*^{CreERT2};*Rosa*^{YFP} mice (MuSC^{YFP}). In this model, tamoxifen administration at 3-5 months of
119 age irreversibly labels Pax7-expressing MuSCs. YFP^{+} cells were isolated at young (3-5 months),
120 middle (10-14 months) and geriatric (>28 months) ages, using a conventional surface markers and
121 gating strategy: stem cell antigen-1 negative (SCA-1^{-}) and vascular cell adhesion protein 1 positive
122 (VCAM1^{+}) cells among lineage negative (CD31^{-}/CD45^{-}) and live cells (Liu et al., 2015) (Fig. 1A).
123 As previously reported, the number of VCAM1^{+}/SCA-1^{-} MuSCs declined significantly with age,
124 from an average of 12.22% at young and 13.62% at middle age to 8.31% at geriatric age (Fig. 1B).
125 The variability of VCAM1^{+} MuSC number at geriatric age likely reflects mouse-to-mouse
126 differences in the onset and progression of late-life phenotypes. Despite this heterogeneity, the
127 overall shift toward a VCAM1-low state was observed across all geriatric replicates. Interestingly,
128 however, when MuSCs were defined by YFP expression alone, their number remained comparable
129 across ages (Fig. 1C). The broader spread observed in the young group likely reflects the known
130 heterogeneity of MuSCs in early adulthood, which encompass multiple transcriptional and
131 functional substates (Dong Seong Cho, 2017). This developmental heterogeneity results in greater
132 variability in young mice compared to the more uniform profiles seen in middle-aged. Although
133 the young group displayed greater biological variability, the overall mean MuSC frequencies were
134 comparable among age groups.
135
136 To investigate the disparity in the numbers of surface marker labelled MuSCs and genetically
137 labelled MuSCs at geriatric age, we examined the expression of traditional MuSC surface markers,
138 VCAM1 and integrin alpha 7 (ITGA7) in YFP^{+} population (Blanco-Bose et al., 2001, Sacco et al.,

139 2008). We observed a significant decline in VCAM1 expression, while ITGA7 expression
140 remained comparable (Fig. 1D). Notably, both VCAM1 and ITGA7 expression showed
141 significantly greater variation at geriatric age, in YFP^+ cells, likely due to inter-individual
142 variability during aging. In young and middle-aged muscle, the $VCAM1^{low}$ and $VCAM1^-$ MuSC
143 populations were extremely small and often nearly absent, indicating that these subsets may be not
144 a substantial component of the MuSC pool earlier in life. The detectable emergence and expansion
145 of $VCAM1^{low}$ cells occurred predominantly at the geriatric stage, suggesting that this population
146 represents an aging-associated state rather than a pre-existing subset.
147
148 Since YFP^+ cells at geriatric age have varying marker gene expression, we investigated their
149 localization *in vivo* by conducting immunohistochemistry of *tibialis anterior* (TA) muscle sections
150 for PAX7. YFP^+ cells showed sublaminar localization and co-expressed PAX7 in middle aged
151 mice (Fig. 1E). In geriatric aged mice, however, the number of $PAX7^+/YFP^+$ cells decreased, while
152 $YFP^+/PAX7^{low/-}$ cells concomitantly increased (Fig. 1E).
153
154 To examine the relationship between PAX7 and varying MuSC marker expression, YFP^+ cells
155 were grouped by VCAM1 expression levels: $VCAM1^{High}$, $VCAM1^{Low}$, and $VCAM1^-$, and
156 immunostained for PAX7. The PAX7 fluorescence intensity was comparable between $VCAM1^{High}$
157 cells from middle-aged and geriatric mice, but was markedly reduced in $VCAM1^{Low}$ and $VCAM1^-$
158 cells of geriatric mice (Fig. 1F). Together, these findings show an emerging population of YFP^+
159 cells that lose traditional markers like Pax7 and VCAM1 at geriatric age.
160
161 *$YFP^+/VCAM1^-$ cells are quiescent MuSCs*

162 To further explore the characteristics of $YFP^+/VCAM1^-$ cells in geriatric mice, we examined their
163 potential myogenic status. Given that loss of canonical markers might reflect lineage progression,
164 we assessed the expression of myogenin (MYOG), a marker of late-stage myogenic differentiation,
165 in YFP^+ cells from uninjured middle, geriatric ages and 5-days post injury. We found that MYOG
166 expression was largely absent in YFP^+ cells from uninjured aged muscle, even in geriatric
167 $YFP^+/VCAM1^{Low}$ and $YFP^+/VCAM1^-$ cells (Fig. 2A-C). This contrasts with robust MYOG signal
168 detected at 5 days post injury, suggesting that YFP^+ cells are not committed myoblasts.
169
170 To further investigate cell identity, we performed single-cell transcriptome analysis of YFP^+ cells
171 from middle-aged and geriatric mice and integrated these data into public single-cell sequencing
172 data of uninjured and injured muscles.(De Micheli et al., 2020, Oprescu et al., 2020) (Fig. S1A-E).
173 Integration of public single-cell sequencing data yielded 5 clusters: quiescent MuSC, activated
174 MuSC, myoblast/myocyte, fast fiber myonuclei and slow fiber myonuclei (Fig. 2D). The
175 transcriptional signatures characterizing each cluster were consistent with known lineage identities,
176 supporting the validity of the clustering (Fig. 2E). High levels of myonuclei transcripts likely
177 represents fragmented myonuclei or cells with compromised nuclear integrity, which is a known
178 technical byproduct of dissociation of the myofiber (Santos et al., 2021). Only high-confidence
179 MuSC clusters were included in differential expression, trajectory inference, and cluster-
180 proportion analyses. All YFP^+ cells from both middle and geriatric age mapped to transcriptional
181 clusters associated with quiescent MuSCs (Fig. 2F). This suggests that even $VCAM1^{Low}$ and
182 $VCAM1^-$ cells from geriatric age did not cluster with activated MuSCs or differentiating myoblasts
183 or myocytes, but rather remained within the quiescent MuSC compartment. These findings support

184 the possibility that these cells may retain core stem-like features, despite altered surface marker
185 profiles.
186
187 Since quiescent MuSCs are generally smaller than activated progenitors due to reduced
188 cytoplasmic volume, low metabolic activity, and compact chromatin organization(Liu et al., 2013),
189 we also compared the cell size of VCAM1^{-} cells with activated MuSCs from injured mice. Indeed,
190 both VCAM1^{Low} and VCAM1^{-} cells from geriatric mice were similar in diameter to YFP^{+} cells
191 from uninjured middle-aged mice, but were significantly smaller than activated MuSCs from
192 injured mice (Fig. S2A-B). These results are consistent with our interpretation that VCAM1^{Low}
193 and VCAM1^{-} cells from geriatric mice may remain in a quiescent state.
194
195 Given reports of smooth muscle mesenchymal cells (SMMCs) expressing overlapping surface
196 markers with MuSCs, we considered whether the VCAM1^{-} cells might reflect SMMC
197 contamination(Giordani et al., 2019). mRNA sequence analysis revealed that this population
198 exhibited low expression of SMMC markers, including Myl9, Acta2, and Pdgfrb (Fig S2C),
199 suggesting they are transcriptionally distinct from SMMCs. VCAM1^{-} cells showed significantly
200 higher Pax7 expression compared to SMMCs. Together, these results suggest that YFP^{+}/VCAM1^{-}
201 cells from geriatric age may retain quiescent features and myogenic identity, despite lacking
202 typical MuSC markers.
203
204 *Impaired functionality of YFP^{+}/VCAM1^{-} MuSCs*
205 Since YFP^{+}/VCAM1^{-} cells retained molecular and morphological features consistent with
206 quiescent MuSCs, we next investigated their functional potential. Colony-forming assays revealed

207 that YFP^{+}/VCAM1^{High} cells from geriatric mice expanded at comparable rates to those from
208 middle-aged mice. In contrast, colony formation by YFP^{+}/VCAM1^{Low} and YFP^{+}/VCAM1^{-} subsets
209 were progressively reduced, with the VCAM1^{-} subsets forming smaller colonies (Fig. 3A-B).
210 These findings suggest that these cells retain proliferative ability, although their expansion
211 capacity was compromised.
212
213 To examine their regenerative potential *in vivo*, we transplanted equal numbers of YFP^{+} cells from
214 each group into pre-injured TA of MuSC-deficient *Pax7^{CreERT2};Rosa^{DTA}* recipient mice (Fig. 3C).
215 In the absence of donor cells, regeneration was severely impaired, consistent with a lack of
216 endogenous MuSCs (Fig 3D). Transplantation of YFP^{+}/VCAM1^{High} cells from both middle-aged
217 and geriatric donors supported robust regeneration, resulting in centrally nucleated myofibers with
218 comparable morphology between age groups, consistent with heterotypic transplantation studies
219 (Fig. 3D-E) (Ikemoto-Uezumi et al., 2015). Interestingly, both YFP^{+}/VCAM1^{Low} or
220 YFP^{+}/VCAM1^{-} cells were also capable of contributing to myofiber regeneration, despite lacking
221 traditional MuSC markers (Fig. 3E). However, regenerated myofibers in these groups were
222 significantly smaller than those derived from VCAM1^{High} cells (Fig. 3F), suggesting that loss of
223 VCAM1 expression may be associated with diminished regenerative capacity.
224
225 Together, these results indicate that even the most marker-deficient MuSCs in geriatric muscle,
226 YFP^{+}/VCAM1^{-} cells, retain a degree of regenerative competence. However, their reduced
227 proliferative output and attenuated *in vivo* contribution suggests functional heterogeneity within
228 the aged MuSC pool, wherein diminished marker expression may correlate with impaired
229 regenerative performance.

230

231 *VCAM1⁻ MuSCs exhibit senescence-like features and sensitivity to senolytics*

232 To investigate the molecular basis of impaired function in VCAM1^{-} MuSCs, we performed mRNA
233 sequence analysis on YFP^{+} MuSCs. Samples showed high quality and a strong correlation was
234 observed among biological replicates (Fig. S3A-C). Each group consistently reproduced similar
235 gene expression patterns in biological replicates in hierarchical clustering (Fig. S3D). Although
236 mid-aged VCAM1-high MuSCs did not exhibit the emergence of a VCAM1-low state, mRNA
237 profiling revealed detectable transcriptional differences between mid-aged and geriatric VCAM1-
238 high populations (Fig. S3D). These shifts likely reflect the gradual accumulation of aging-
239 associated molecular changes that begin during the middle-aged stage, even before overt functional
240 decline or loss of VCAM1 becomes evident. Importantly, these early transcriptomic alterations do
241 not give rise to the dysfunctional VCAM1-low subset, which emerges only in geriatric muscle. In
242 particular, hierarchical clustering showed similar gene expression pattern between VCAM1^{High}
243 MuSCs of middle-aged and geriatric mice and between VCAM1^{Low} and VCAM1^{-} MuSCs (Fig.
244 S3E), consistent with our results of *in vivo* and *in vitro* functionality experiments (Fig. 3A-F).

245

246 Kyoto-encyclopedia of genes and genomes (KEGG) pathway enrichment analysis based on the
247 DEGs (Fig. S3E) (Kolberg et al., 2023) showed alterations in pathways related to cellular
248 senescence and PI3K-AKT pathway in VCAM1^{-} MuSCs of geriatric age as compared to
249 VCAM1^{High} MuSCs of middle-age (Fig. 4A). We further investigated the expression levels of
250 individual genes known to be altered in MuSCs of aged mice, such as genes related to extracellular
251 matrix (Schuler et al., 2021), Notch signaling (Liu et al., 2018, Conboy et al., 2003, Conboy et al.,
252 2005), and autophagy-lysosomal pathway (Garcia-Prat et al., 2016, Kim et al., 2021b), some of

253 which were more altered in VCAM1^{Low} and VCAM1^{-} MuSCs compared to VCAM1^{High} MuSCs
254 of geriatric mice (Fig. 4B). *Cdkn2a* (*p16^{INK4a}*) and *Cdkn2b* (*p15^{INK4b}*), which are cell cycle
255 regulators widely used as markers for senescent cells, showed highly altered expression patterns
256 in VCAM1^{-} MuSCs compared to VCAM1^{Low} MuSCs (Fig. 4B) (Saito and Chikenji, 2021).
257 However, the expression levels of other well-known cellular senescence marker genes, such as
258 *Rb1*, *Il6*, and *Trp53*, were not altered much. *Pik3cb* and *Tsc1,* which are involved in the PI3K-Akt-
259 mTOR pathway, showed overall increased expression, while other genes in the PI3K-Akt pathway
260 remained relatively unchanged. Together, these results suggest a unique combination of *in vivo*
261 senescence-like molecular characteristics of VCAM1^{-} MuSCs, distinct from molecular
262 characteristics of replicative cellular senescence.
263
264 Given their unique senescence associated transcriptome and partially elevated PI3K-Akt pathway,
265 we tested whether VCAM1^{-} MuSCs were susceptible to senolytic elimination. Geriatric mice were
266 treated with senolytic agents dasatinib and quercetin (DQ) (Xu et al., 2018), and analyzed 2 weeks
267 later (Fig. 4C). Despite variation in baseline VCAM1^{High} and VCAM1$^{Low/-}$ population across aged
268 animals, a consistent inverse correlation was observed between VCAM1^{High} and VCAM1$^{Low/-}$
269 fractions (Fig. S3F). The multimodal distribution observed in the geriatric group reflects increased
270 mouse-to-mouse variability that emerges at very advanced ages. Following DQ treatment,
271 VCAM1^{High} MuSCs remained comparable while VCAM1$^{Low/-}$ MuSCs showed reduced abundance
272 and lower variability ($p = 0.0596$) (Fig. 4D). The multimodal distribution observed in the geriatric
273 group reflects increased mouse-to-mouse variability that emerges at very advanced ages. Although
274 aging affects all animals, the extent and timing of phenotypic changes vary substantially among
275 individuals, resulting in broader divergence in VCAM1 expression states. Statistical analyses were

276 performed using the mouse as the biological replicate, this variability does not alter the overall
277 conclusion. These results indicate selective sensitivity of VCAM1$^{Low/-}$ MuSCs to senolytic agents
278 and their increased dependence on BCL-2–related survival pathways.
279
280 Together, our findings reveal a distinct subset of quiescent MuSCs in geriatric muscle that exhibit
281 unique senescence-like molecular features and are amenable to senolytic clearance. We term these
282 cells GERI-MuSCs (Geriatric Emerging Regeneration-capable and Impaired-MuSCs).
283
284 *Rejuvenation of GERI-MuSCs by DHT treatment*
285 Studies have demonstrated that treatment with rejuvenating agents can restores myofiber
286 regeneration capacity in aged mice (Bernet et al., 2014, Cosgrove et al., 2014, Zhang et al., 2016,
287 Elabd et al., 2014, Price et al., 2014, Garcia-Prat et al., 2016). Previously, dihydrotestosterone
288 (DHT) supplementation has been shown to preserve MuSCs function and enhance regeneration in
289 Antide, a GnRH antagonist, treated mice by restoring autophagy activation (Kim et al., 2021b).
290 Consistent with these findings, implantation of DHT-filled silastic tube in 28-month-old geriatric
291 mice improved muscle regeneration, as evidenced by increased fiber cross sectional area (Fig.
292 S4A-C).
293
294 To investigate whether DHT could affect GERI-MuSCs, we treated 28-month-old MuSC^{YFP} mice
295 with DHT and analyzed MuSC populations one month later (Fig. 4E). Remarkably, DHT treatment
296 resulted in a decrease in GERI-MuSCs with a corresponding expansion of VCAM1^{High} MuSCs
297 population. This phenotypic reversion suggests that DHT promotes restoration of canonical marker
298 expression in GERI-MuSCs.

299

300 To determine whether DHT acts through rejuvenation of GERI-MuSCs, we first treated the mice
301 with DQ for 5 consecutive days and then implanted DHT tube 2 weeks later (Fig. 4F). In mice pre-
302 treated with DQ, DHT supplementation failed to reconstitute the VCAM1^{High} MuSC pool (Fig.
303 4F). This finding suggests a model in which GERI-MuSCs are not terminally senescent, but rather
304 exist in a latent, hormone-responsive state. Upon DHT exposure, these cells likely reacquire a
305 VCAM1^{High} phenotype, underscoring their potential as a therapeutic target in muscle aging.

306

307 *Identification of GERI-MuSCs using CD63 and CD200*

308 In non-reporter models, the detection and isolation of GERI-MuSCs pose a significant challenge,
309 as these cells lack expression of conventional MuSC markers such as VCAM1 and PAX7 at
310 geriatric age. To overcome this limitation, we conducted a transcriptomic screen to identify
311 alternative surface markers that remain stably expressed across the full spectrum of MuSC aging
312 states. Candidate genes were selected based on three criteria; high transcript abundance (RPKM),
313 consistent expression from VCAM1^{High} to VCAM1^{-} MuSCs, and predicted surface localization
314 (Fig. 5A). CD63 and CD200 sufficed all three criteria and were therefore chosen as candidate
315 markers for further validation (Fig. 5B).

316

317 We confirmed protein level expression of CD63 and CD200 expression in MuSCs by co-
318 immunostaining TA cross-sections for CD63, CD200, YFP and PAX7. Both markers co-localized
319 with YFP and PAX7 beneath the basal lamina (Fig. 5C). Flow cytometry analysis further
320 demonstrated that 96.3% of YFP^{+}/VCAM1^{+} cells from young MuSC^{YFP} mice were
321 CD63^{high}/CD200^{high} (Fig. 5D). Notably, among lineage-negative (CD31^{-}/CD45^{-}), SCA-1^{-}, and

322 live cells, 93.2% of CD63^{high}/CD200^{high} cells were YFP^{+}/VCAM1^{+} cells (Fig. 5E). Importantly,
323 96.5±2.8% of sorted CD63^{high}/CD200^{high} cells were PAX7^{+}, validating these markers as a robust
324 strategy for MuSC enrichment.
325
326 To assess whether the CD63/CD200-based strategy could detect and isolate GERI-MuSCs in wild-
327 type mice, we applied the strategy to middle and geriatric aged mice. In middle aged mice, all
328 CD63^{high}/CD200^{high} cells corresponded exclusively to VCAM1^{High} MuSCs (Fig. 5F). In contrast,
329 geriatric mice exhibited a marked shift, with the majority of CD63^{high}/CD200^{high} cells falling
330 within the VCAM1$^{Low/-}$ gate (Fig. 5F). These results indicate that CD63 and CD200 expression is
331 preserved in GERI-MuSCs, enabling their prospective identification and isolation in the absence
332 of genetic labeling. Therefore, these findings establish CD63 and CD200 as reliable surface
333 markers that can be used with VCAM1. Together, they can to detect the full spectrum of MuSCs,
334 including functionally latent populations that evade detection by conventional means. This strategy
335 offers a critical tool for future studies aiming to comprehensively characterize MuSC heterogeneity
336 and therapeutic responsiveness in the context of aging.
337
338 **Discussion**
339 Our study challenges the longstanding paradigm that muscle stem cell (MuSC) number declines
340 irreversibly with age. While previous reports have described significant depletion of Pax7^{+} MuSCs
341 in aged muscle, these findings were largely based on immunohistochemical detection or flow
342 cytometric profiling using conventional surface markers. Here, we demonstrate that genetically
343 labeled MuSCs, tracked longitudinally *in vivo* using a Pax7-CreERT2;Rosa-YFP model, do not
344 decrease in number even in geriatric mice. Instead, a substantial subset of aged MuSCs loses

345 expression of canonical markers such as Pax7 and VCAM1, rendering them undetectable by
346 traditional approaches. Although VCAM1 is frequently used as a surface marker for MuSC
347 identification, it represents only one of several commonly used markers, and ITGA7-based
348 strategies remain widely applied in the field. In our dataset, ITGA7 expression within the YFP^+
349 MuSC population did not show a significant reduction in mean fluorescence with aging (Fig. 1D).
350 However, the variance of ITGA7 expression was markedly increased in geriatric MuSCs,
351 indicating greater phenotypic heterogeneity. This pattern suggests that aging does not uniformly
352 downregulate canonical markers but instead increases instability and variability in their expression,
353 which may lead to under-detection of a subset of MuSCs even when ITGA7 is used as the primary
354 gating marker. These findings underscore that marker-based quantification may underestimate
355 specific aging-associated MuSC subpopulations and should be interpreted within this limitation.
356
357 We identify this overlooked population as GERI-MuSCs (Geriatric Emerging Regeneration-
358 capable and Impaired MuSCs). Despite their diminished expression of hallmark MuSC markers,
359 GERI-MuSCs exhibit features consistent with quiescence, rather than terminal differentiation or
360 apoptosis. Although GERI-MuSCs showed markedly reduced colony formation and further
361 validation using direct viability assays are necessary, several lines of evidence suggest that they
362 are viable rather than acutely undergoing cell death. These cells can be isolated as intact
363 populations by FACS and generate high-quality RNA-sequencing libraries, which would not be
364 feasible if they were non-viable. Their transcriptomic profiles also show enrichment of stress-
365 response and senescence-associated programs rather than apoptotic signatures. Together, these
366 findings suggest that GERI-MuSCs remain alive but exhibit impaired proliferative capacity.
367 Furthermore, transcriptomic profiling and functional assays reveal that these cells retain a partial

368 capacity for proliferation and regeneration, albeit at reduced efficiency. When comparing geriatric
369 VCAM1^{+} MuSCs with middle aged MuSCs, we found 1,428 DEGs, where 701 genes were
370 downregulated and 727 genes were upregulated (Fig. S3E). Some of the pathways altered were
371 similar to previously reported differences, such as alterations in the autophagy-lysosome related
372 genes and PI3K-Akt Pathways (Garcia-Prat et al., 2016). However, these transcriptomic alterations
373 did not affect the functional integrity of geriatric VCAM1^{+} MuSCs (Fig. 3 A-F). Taken together,
374 these results do not contradict prior studies demonstrating age-related MuSC decline but rather
375 refine this understanding by highlighting a subset of aged MuSCs that may have been
376 underrepresented or more difficult to detect using conventional markers. By resolving these cells
377 with an alternative phenotypic definition, our findings complement existing models of MuSC
378 aging and suggest that part of the apparent depletion previously reported may reflect changes in
379 marker expression rather than complete cellular loss.
380
381 GERI-MuSCs display a unique gene expression profile that includes upregulation of senescence-
382 associated transcripts such as *Cdkn2a* but unaltered expression of other typical senescence-
383 associated genes, such as *Il6* and *Trp53*, while showing preservation of certain stemness-related
384 pathways (Fig. 4B). These cells do not fulfill the classical definition of cellular senescence, such
385 as irreversible cell cycle arrest(Campisi and d'Adda di Fagagna, 2007). p16 expression is elevated
386 in VCAM-low MuSCs, but this alone does not establish a fully senescent state. Rather, GERI-
387 MuSCs exhibit a hybrid state of retaining regenerative potential while expressing select markers
388 traditionally associated with senescence. This finding suggests that the criteria used to define
389 senescence in proliferative cell types may not fully apply to quiescent stem cells like MuSCs,
390 which spend most of their life in a non-proliferative state. Additional markers and functional assays

391 will be needed to define the precise state of these cells and to delineate *in vivo* senescence features
392 specific to long-lived, tissue-resident stem cells.
393
394 Our results suggest that GERI-MuSCs could be functionally reactivated. Treatment with
395 dihydrotestosterone (DHT) restored VCAM1 expression in GERI-MuSCs and regenerative
396 performance in aged mice, suggesting that their phenotype is reversible and hormonally responsive.
397 This provides a compelling explanation for the efficacy of hormone-based interventions in aging
398 muscle and highlights the potential for targeting latent regenerative capacity in aged stem cells.
399 Notch signaling appears to be a key regulator of this reversible phenotype. We found diminished
400 expression of Notch pathway components, including Notch1, Notch3, Hey1, and HeyL, in
401 $VCAM1^{Low}$ and $VCAM1^{-}$ subsets, along with reduced transcription of Pax7 and VCAM1. Given
402 that both Pax7 and VCAM1 are downstream targets of Notch signaling and that Notch activity can
403 be modulated by androgen signaling, the restoration of MuSC function by DHT may act through
404 this axis. Testing such mechanisms in future studies will be important for establishing therapeutic
405 strategies.
406
407 Although DHT supplementation partially restored the regenerative performance of geriatric
408 MuSCs, this effect cannot be attributed solely to the rescue of VCAM1 expression in GERI-
409 MuSCs. Androgen signaling is known to influence multiple non–stem cell populations in the
410 muscle environment, including fibro-adipogenic progenitors, myofibers, and immune cells, any of
411 which may contribute to the observed improvement in regeneration (Kim et al., 2021b).
412 Accordingly, we acknowledge that DHT likely exerts broader tissue-level effects beyond the
413 MuSC compartment, and our findings should be interpreted within this limitation. Future studies

414 combining senolytic strategies with targeted modulation of androgen signaling may help delineate
415 the relative contributions of each pathway, although such experiments extend beyond the scope of
416 the present work.
417
418 The presence of GERI-MuSCs also raises caution about the use of senolytic agents. Although
419 dasatinib and quercetin are used to clear senescent cells and have shown benefits in aged tissue,
420 our data show that these agents also deplete GERI-MuSCs. Since GERI-MuSCs retain
421 functionality and regenerative potential, their removal could compromise muscle maintenance and
422 repair in elderly individuals. Given the critical role of MuSCs in preserving muscle mass,
423 supporting myonuclei turnover, and maintaining neuromuscular junctions, the long-term
424 application of senolytics in skeletal muscle warrants careful scrutiny.
425
426 Finally, we propose CD63 and CD200 as reliable surface markers that can be used with VCAM1
427 for identifying MuSCs across age groups. These markers remain expressed in both young and aged
428 MuSCs, including those with diminished canonical marker expression. CD63 and CD200
429 expression in geriatric muscle was evaluated using conventionally isolated MuSCs rather than
430 YFP-traced cells. This distinction should be considered when interpreting these results. Their use
431 enables comprehensive isolation of the full MuSC population and will be instrumental in
432 improving the resolution of future studies on stem cell heterogeneity and aging.
433
434 In conclusion, we identify a previously unrecognized population of MuSCs—GERI-MuSCs—that
435 persists with age despite loss of conventional markers. These cells remain quiescent, partially
436 functional, and responsive to rejuvenation cues. Their discovery challenges existing models of

437 MuSC depletion and senescence, and underscores the importance of revisiting stem cell aging with
438 improved detection strategies and nuanced interpretations of cellular function.

439 **Materials and Methods**

440 ***List of Antibodies for Flow Cytometry and FACS (Fluorescence-activated cell sorting***

Marker	Fluorophore	Catalog No.	Company
CD31	APC	102510	BioLegend
CD31	Pacific Blue™	108120	BioLegend
CD45	APC	103112	BioLegend
CD45	Pacific Blue™	405206	BioLegend
VCAM1	Biotin	553331	BD Biosciences
Streptavidin	PE/Cy7	405206	BioLegend
Ly-6A/E (Sca-1)	Pacific Blue™	108120	BioLegend
Ly-6A/E (Sca-1)	FITC	553335	BD Biosciences
CD200	BV711	745548	BD Biosciences
CD63	APC	170631-82	eBioscience

441

442 ***Animals***

443 All animal procedures conformed to the guidelines of Institutional Animal Care and Use
444 Committee (IACUC) of Seoul National University, Korea. Male C57BL/6J mice were housed
445 under a 12-h light/12-h dark cycle at 22°C with 40-60% humidity, and fed ad libitum. $Pax7^{CreER}$
446 (017763), $Rosa^{YFP}$ (006148), $Rosa^{DTA}$ (009669) mice were obtained from the Jackson Laboratory
447 (Bar, Harbor, ME, USA). Tamoxifen (25mg/mL in corn oil; Sigma-Aldrich, St. Louis, MO, USA)
448 was administered orally for 5 consecutive days (240 mg/kg). For muscle injury, mice were
449 anesthetized with avertin (250 μg/g, i.p.) and injected with 60 μL of 1.2% BaCl2 (Sigma-Aldrich)

450 into the Tibialis Anterior (TA) muscles. One-day post-injury, mice were anesthetized with avertin
451 and MuSCs were transplanted at indicated numbers.
452
453 ***Flow Cytometry and FACS (Fluorescence-activated cell sorting)***
454 Limb muscles were mechanically dissected and enzymatically dissociated in Dulbecco's modified
455 Eagle's medium (DMEM) containing 10% horse serum (Hyclone, Logan, UT, USA), collagenase
456 type II (800U/mL; Worthington, Lakewood, NJ, USA), and dispase (1.1 U/mL; StemCell
457 Technologies, Vancouver, BC, Canada) at 37°C for 50 minutes. Digested suspensions were
458 triturated, washed with DMEM and filtered to obtain mononuclear cells. Cells were stained with
459 antibodies, analyzed and sorted using a FACS Aria III or FACS Aria Fusion (BD Bioscience). List
460 of antibodies used are provided as supplementary materials. For all flow cytometry analyses, fibro-
461 adipogenic progenitors (FAPs) were excluded by gating out $Sca1^{+}CD31^{-}CD45^{-}$ cells prior to
462 MuSC identification. This strategy ensured that YFP^{+} MuSC quantification was not confounded
463 by age-associated changes in $Sca1^{+}$ mesenchymal populations. Representative plots were
464 processed with FlowJo v10.9.
465
466 ***MuSC Culture***
467 FACS-isolated MuSCs were cultured in DMEM/F12 + 20% FBS + 1% ZellShield (Minerva
468 Biolabs, Germany) + 2.5 ng/mL bFGF (F0291, Sigma Aldrich) on Matrigel (256231, BD
469 Bioscience)-coated plates at 37°C and 5% CO_2. Medium was refreshed every 3 days. MuSCs were
470 imaged daily using EVOS FL Auto 2 (Thermo Fisher, USA) and the number of cells in the same
471 region was counted.
472

473 ***Histochemistry and Immunohistochemistry***

474 TA muscles were fixed overnight in 4% paraformaldehyde, embedded in the Tissue Tek OCT
475 compound (Sakura Fineteck, USA), and snap-frozen in liquid nitrogen. The muscles were
476 sectioned at 7μm and stained on the slides. H&E staining was performed according to basic
477 protocols. For immunostaining, sections were subjected to epitope retrieval in 50mM Tris-EDTA
478 (pH 9.0) at 105°C for 10 minutes, then blocked with 3% BSA + 0.1% Triton X-100. Sections were
479 incubated overnight with primary antibodies, mouse anti-PAX7 (DSHB, Pax7, 1:100 dilution),
480 chicken anti-GFP (abcam, ab13970, 1:300), rabbit anti-laminin (Sigma, L9393-2ML, 1:500), rat
481 anti-CD200 (BD Biosciences, 1:50), and rat anti-CD63 (eBioscience, 1:50). After washing,
482 sections were incubated with secondary antibodies, Alexa Fluor 647-conjugated anti-rat or anti
483 rabbit IgG, Alexa Fluor 594-conjugated anti mouse IgG, and Alexa Fluor 488-conjugated anti
484 chicken IgG. Nuclei were counterstained with Hoechst 33342 (Invitrogen, H3570). Slides were
485 mounted with VECTASHIELD (Vector Laboratories) and images were acquired using EVOS FL
486 Auto 2 (Thermo Fisher) and Leica TCS SP8 confocal microscope. Cross-sectional area (CSA) was
487 calculated by SMASH[23] and ImageJ programs, respectively.

488

489 ***Immunocytochemistry***

490 Isolated MuSCs were cytospun onto slides (Cytospin 4, Thermo Scientific), fixed with 4%
491 paraformaldehyde for 10 minutes, washed with PBS and permeabilized with PBS containing 0.4%
492 Triton X-100 for 30 minutes. Slides were then incubated with primary antibodies, mouse anti-
493 PAX7 (DSHB) and mouse anti-MYOG (DSHB, F5D, 1:100 dilution) in blocking buffer.
494 Subsequent steps followed the immunohistochemistry protocol. Relative fluorescent intensity was
495 quantified using ImageJ.

496

497 ***Senolytics and DHT treatment***

498 Dihydrotestosterone (DHT) implantation was performed as previously described[8]. Senolytic
499 agents Dasatinib (D-3307, LC laboratories, 5mg/kg) and Quercetin (Q4951, Sigma, 50 mg/kg) was
500 administered orally for 5 consecutive days. Experimental schemes of combined treatment are as
501 mentioned in the results section of this article.

502

503 ***Single-cell RNA sequence analysis***

504 To obtain gene-specific UMI (Unique Molecular Identifier) counts in each cell, we processed raw
505 scRNA-seq data using the BD Rhapsody WTA analysis pipeline (v1.11.1)[24]. Scanpy (v1.9.3)[25]
506 was utilized for single-cell RNA sequence analysis. Cells with a gene count below 200 or a
507 mitochondrial gene percentage above 20% were considered low-quality cells and were excluded
508 from downstream analyses. We set the upper limit of each UMI count as (mean(total counts) + 2
509 standard deviation(total counts) value) to remove doublets. Normalization was applied to the count
510 matrix (scanpy.pp.normalize_total with target_sum=10^4 and scanpy.pp.log1p).

511 We characterized the enriched cells by merging our scRNA-seq data with public datasets
512 (GSE162172, GSE138826)[26,27]. From the public dataset, only the cells belonging to the
513 myogenic lineage (from quiescent MuSCs to Myonuclei (Type IIb or IIx)) were selected for
514 comparison. After merging the public dataset with our dataset
515 (scanpy.external.pp.harmony_integrate with max_iter_harmony=50), 2000 highly variable genes
516 were identified and scaled (scanpy.pp.highly_variable_genes with n_top_genes=2000,
517 scanpy.pp.scale with max_value=10).

518 We visualized the scRNA-seq data using uniform manifold approximation and projection (UMAP)
519 (scanpy.tl.umap) with a precomputed neighborhood graph (scanpy.pp.neighbors with n_pcs=50).
520 We clustered the UMAP-transformed data using the Louvain algorithm (scanpy.tl.louvain,
521 resolution=0.5). Each cluster was annotated using cell-specific markers (Fig. 1D, E). The
522 proportions of quiescent MuSCs, activated MuSCs, and Myoblasts/Progenitors were measured in
523 our samples (Mid and Geri) and the public dataset across various days-post-injury (DPI). Cases
524 with less than 50 cells per DPI were excluded during this analysis (Fig. S1A).
525 We utilized diffusion map, PAGA, and force-directed graph to analyze the trajectory of cells
526 belonging to the myogenic lineage. After dimension reduction using diffusion maps
527 (scanpy.tl.diffmap), we computed neighborhood graphs (scanpy.pp.neighbors) and abstracted the
528 graphs using PAGA (scanpy.tl.paga). We modeled the trajectory of the cells using the abstracted
529 graphs as initial positions by constructing a force-directed graph (Fig. S1B-E).
530
531 ***Representative Isoforms of Mouse mRNAs***
532 To acquire a sole representative isoform for each gene, we utilized the filtering pipeline described
533 in a previous study(Kim et al., 2016). The mouse reference annotation (GRCm39 refFlat) was
534 downloaded from the UCSC website(Pruitt et al., 2007). mRNA sequences with accession
535 category 'NM' located on the 21 chromosomes (1-19, X, and Y) were selected for downstream
536 analyses. Entries with incorrect start or stop codons, internal stop codons, and ORF lengths not
537 divisible by 3, were removed. Nonsense-mediated mRNA decay candidates, defined as the
538 mRNAs with stop codons positioned less than 50 nucleotides before the final exon-exon junction,
539 were excluded (Nagy and Maquat, 1998). A total of 20,582 non-redundant representative isoforms
540 were selected as mouse reference mRNAs for subsequent analyses.

541

542 ***mRNA sequence analysis***

543 mRNA sequence analysis was performed on 3-4 biological replicates for each condition. We
544 trimmed low-quality read ends using a custom algorithm. Each base position was assigned a
545 reward (+5) or a penalty (-1) based on its Phred score with a threshold of 30. To define high-quality
546 read ends, we calculated the cumulative sum from both ends, identified the positions with the
547 minimum value, and trimmed the reads at those positions. This process was repeated iteratively
548 until no further trimming was necessary. Reads shorter than 17 bases after trimming were excluded.
549 Subsequently, we removed adapter sequences using Cutadapt (v3.1) (Martin, 2011) with options
550 (-O 10 -m 18 --match-read-wildcards). We eliminated sequencing artifacts and PCR duplicates
551 using FASTX-Toolkit's fastx_artifact_filter with option (-Q 33) (hannonlab.cshl.edu/fastx_toolkit/,
552 v0.0.13). To eliminate reads derived from mouse non-coding RNA, we aligned the reads to non-
553 coding RNA sequences in RNAcentral(Consortium, 2021) using Bowtie2 (v2.1.0) (Langmead and
554 Salzberg, 2012) with options (-k 1 --norc --very-sensitive), and the reads aligned to non-coding
555 RNAs were excluded. Unpaired reads were also excluded.

556 Preprocessed reads were aligned to the mouse genome (GRCm39) utilizing the STAR alignment
557 software (v2.7.5b) (Dobin et al., 2013). The parameters used for the STAR alignment are described
558 in a previous study (Kim et al., 2021a). The reads were sorted and indexed using Samtools (v0.1.19)
559 (Danecek et al., 2021). The expression of each gene was quantified by calculating the fragment
560 per kilobase of transcript per million mapped reads (FPKM).

561 We applied the same analysis pipeline to both our experimental samples (Mid, V^H, V^L, V^-) and
562 publicly available SMMC samples (GSE110878, SRR67542132-SRR67542134)(Giordani et al.,

563 2019) to calculate gene expression levels. Quantile-normalized expression levels were compared
564 between the two datasets (Fig. S2C).
565 The following analyses were performed exclusively on our experimental samples.
566 To assess the quality of our samples, the proportion of reads that were either removed, unmapped,
567 or successfully mapped was computed for each sample throughout the preprocessing and
568 alignment steps (Fig. S3B). The correlation between replicates was quantified using Spearman's
569 R (Fig. S3C).
570 We normalized all samples using the following procedure to ensure a fair inter-sample comparison.
571 We applied quantile normalization to equalize the FPKM distribution of all samples. To remove
572 individual mouse variations, we used the RUVs function (k=2) from the RUVSeq package (v1.34.0)
573 (Risso et al., 2014). Subsequently, genes with normalized expression higher than the 50th percentile
574 were selected, and the expression values were z-normalized. We clustered the samples using the
575 clustermap function of the Seaborn package (v0.11.1) (Waskom, 2021) with correlation metric
576 (Fig. S3D).
577 We identified differentially expressed genes (DEGs) by comparing the expression between the
578 Mid, V^H, V^L, and V^- samples. We used DESeq2 (v1.40.2) (Love et al., 2014) to compute $\log_2$ fold
579 changes and false discovery rate (FDR) corrected Q values for individual genes. DEGs were
580 defined as genes with $|\log_2 \text{ fold change}| > 1.2$ and FDR-corrected Q value < 0.05 (Fig. S3E).
581 To annotate the pathways linked to DEGs, we performed enrichment analysis for Kyoto
582 Encyclopedia of Genes and Genomes (KEGG) pathways using the g:Profiler web server (Kolberg
583 et al., 2023, Kanehisa et al., 2016). Among the highly expressed 12,000 genes, DEGs were queried
584 using the g:GOst tool, and the g:SCS algorithm was employed for multiple testing correction.
585 Pathways with multiple testing corrected Q value < 0.05 were presented (Fig. 3A).

586

587 ***Statistical Analysis***

588 All statistical analyses were performed using R (R-4.3.1) and GraphPad Prism. All variables were
589 confirmed to have a normal distribution by using the Shapiro-Wilk test and Kolmogorov-Smirnov
590 test. For comparison of significant differences in 2 groups of normally distributed data, Levene's
591 test for homogeneity of variance using the car package followed by a 2-tailed Student's *t* test or
592 Welch's *t* test was used. For comparison of multiple groups, one-way analysis of variance
593 (ANOVA) or two-way ANOVA followed by Bonferroni's multiple comparison test was
594 performed. All data are presented as mean ± s.d. n.s., not significant; P > 0.05; *P <0.05; **P<0.01;
595 ***P<0.001, ****P<0.0001. *P value* of <.05 considered statistically significant at the 95%
596 confidence level. The number of biological replicates, *p* values, and detailed statistical method for
597 each data were indicated in the figure legends.

598

599 **Acknowledgments**

600 We thank C. Kang (Seoul National University) for providing senolytic agents, Dasatinib and
601 Quercetin.

602

603 **Funding**

604 This work was supported by the National Research Foundation of Korea (NRF) grant funded by
605 the Korea government (MIST) (RS-2020-NR049538, RS-2025-00556439)

606

607 **Data and materials availability:** The bulk RNA sequencing data and scRNA-seq data have been
608 deposited at Gene Expression Omnibus (GEO, GSE accession number: GSE254475 and

609 GSE254476, respectively) and are publicly available as of the date of publication. Source data
610 supporting the findings of this study are provided with this paper. Additional data that support the
611 findings of this study are available from the corresponding author upon reasonable request.

612 **References**

613 BERNET, J. D., DOLES, J. D., HALL, J. K., KELLY TANAKA, K., CARTER, T. A. & OLWIN, B. B.
614 2014. p38 MAPK signaling underlies a cell-autonomous loss of stem cell self-renewal in skeletal muscle
615 of aged mice. *Nat Med,* 20**,** 265-71.

616 BLANCO-BOSE, W. E., YAO, C. C., KRAMER, R. H. & BLAU, H. M. 2001. Purification of mouse
617 primary myoblasts based on alpha 7 integrin expression. *Exp Cell Res,* 265**,** 212-20.

618 BLAU, H. M., COSGROVE, B. D. & HO, A. T. 2015. The central role of muscle stem cells in regenerative
619 failure with aging. *Nat Med,* 21**,** 854-62.

620 CAMPISI, J. & D'ADDA DI FAGAGNA, F. 2007. Cellular senescence: when bad things happen to good
621 cells. *Nat Rev Mol Cell Biol,* 8**,** 729-40.

622 CARLSON, M. E., CONBOY, M. J., HSU, M., BARCHAS, L., JEONG, J., AGRAWAL, A., MIKELS, A.
623 J., AGRAWAL, S., SCHAFFER, D. V. & CONBOY, I. M. 2009. Relative roles of TGF-beta1 and Wnt in
624 the systemic regulation and aging of satellite cell responses. *Aging Cell,* 8**,** 676-89.

625 CHAKKALAKAL, J. V., JONES, K. M., BASSON, M. A. & BRACK, A. S. 2012. The aged niche disrupts
626 muscle stem cell quiescence. *Nature,* 490**,** 355-60.

627 CONBOY, I. M., CONBOY, M. J., SMYTHE, G. M. & RANDO, T. A. 2003. Notch-mediated restoration
628 of regenerative potential to aged muscle. *Science,* 302**,** 1575-7.

629 CONBOY, I. M., CONBOY, M. J., WAGERS, A. J., GIRMA, E. R., WEISSMAN, I. L. & RANDO, T. A.
630 2005. Rejuvenation of aged progenitor cells by exposure to a young systemic environment. *Nature,* 433**,**
631 760-4.

632 CONSORTIUM, T. R. 2021. RNAcentral 2019: a hub of information for non-coding RNA sequences.
633 *Nucleic Acids Res,* 49**,** D212-D220.

634 COSGROVE, B. D., GILBERT, P. M., PORPIGLIA, E., MOURKIOTI, F., LEE, S. P., CORBEL, S. Y.,
635 LLEWELLYN, M. E., DELP, S. L. & BLAU, H. M. 2014. Rejuvenation of the muscle stem cell population
636 restores strength to injured aged muscles. *Nat Med,* 20**,** 255-64.

637 DANECEK, P., BONFIELD, J. K., LIDDLE, J., MARSHALL, J., OHAN, V., POLLARD, M. O.,
638 WHITWHAM, A., KEANE, T., MCCARTHY, S. A., DAVIES, R. M. & LI, H. 2021. Twelve years of
639 SAMtools and BCFtools. *Gigascience,* 10.

640 DAY, K., SHEFER, G., SHEARER, A. & YABLONKA-REUVENI, Z. 2010. The depletion of skeletal
641 muscle satellite cells with age is concomitant with reduced capacity of single progenitors to produce reserve
642 progeny. *Dev Biol,* 340**,** 330-43.

643 DE MICHELI, A. J., LAURILLIARD, E. J., HEINKE, C. L., RAVICHANDRAN, H., FRACZEK, P.,
644 SOUEID-BAUMGARTEN, S., DE VLAMINCK, I., ELEMENTO, O. & COSGROVE, B. D. 2020. Single-
645 Cell Analysis of the Muscle Stem Cell Hierarchy Identifies Heterotypic Communication Signals Involved
646 in Skeletal Muscle Regeneration. *Cell Rep,* 30**,** 3583-3595 e5.

647 DEGENS, H. 2007. The role of systemic inflammation in age-related muscle wasting and reparation. *J*
648 *Physiol,* 583**,** 343--344.

649 DOBIN, A., DAVIS, C. A., SCHLESINGER, F., DRENKOW, J., ZALESKI, C., JHA, S., BATUT, P.,
650 CHAISSON, M. & GINGERAS, T. R. 2013. STAR: ultrafast universal RNA-seq aligner. *Bioinformatics,*
651 29**,** 15-21.

652 DONG SEONG CHO, J. D. D. 2017. Single cell transcriptome analysis of muscle satellite cells reveals
653 widespread transcriptional heterogeneity. *Gene,* 636**,** 54-63.

654 ELABD, C., COUSIN, W., UPADHYAYULA, P., CHEN, R. Y., CHOOLJIAN, M. S., LI, J., KUNG, S.,
655 JIANG, K. P. & CONBOY, I. M. 2014. Oxytocin is an age-specific circulating hormone that is necessary
656 for muscle maintenance and regeneration. *Nat Commun,* 5**,** 4082.

657 EVANO, B. & TAJBAKHSH, S. 2018. Skeletal muscle stem cells in comfort and stress. *NPJ Regen Med,*
658 3**,** 24.

659 GARCIA-PRAT, L., MARTINEZ-VICENTE, M., PERDIGUERO, E., ORTET, L., RODRIGUEZ-
660 UBREVA, J., REBOLLO, E., RUIZ-BONILLA, V., GUTARRA, S., BALLESTAR, E., SERRANO, A. L.,
661 SANDRI, M. & MUNOZ-CANOVES, P. 2016. Autophagy maintains stemness by preventing senescence.
662 *Nature,* 529**,** 37-42.

663 GIORDANI, L., HE, G. J., NEGRONI, E., SAKAI, H., LAW, J. Y. C., SIU, M. M., WAN, R., CORNEAU,
664 A., TAJBAKHSH, S., CHEUNG, T. H. & LE GRAND, F. 2019. High-Dimensional Single-Cell
665 Cartography Reveals Novel Skeletal Muscle-Resident Cell Populations. *Mol Cell,* 74**,** 609-621 e6.

666 HERNANDO-HERRAEZ, I., EVANO, B., STUBBS, T., COMMERE, P. H., JAN BONDER, M., CLARK,
667 S., ANDREWS, S., TAJBAKHSH, S. & REIK, W. 2019. Ageing affects DNA methylation drift and
668 transcriptional cell-to-cell variability in mouse muscle stem cells. *Nat Commun,* 10**,** 4361.

669 IKEMOTO-UEZUMI, M., UEZUMI, A., TSUCHIDA, K., FUKADA, S., YAMAMOTO, H.,
670 YAMAMOTO, N., SHIOMI, K. & HASHIMOTO, N. 2015. Pro-Insulin-Like Growth Factor-II
671 Ameliorates Age-Related Inefficient Regenerative Response by Orchestrating Self-Reinforcement
672 Mechanism of Muscle Regeneration. *Stem Cells,* 33**,** 2456-68.

673 KANEHISA, M., SATO, Y., KAWASHIMA, M., FURUMICHI, M. & TANABE, M. 2016. KEGG as a
674 reference resource for gene and protein annotation. *Nucleic Acids Res,* 44**,** D457-62.

675 KIM, D., KIM, S., PARK, J., CHANG, H. R., CHANG, J., AHN, J., PARK, H., PARK, J., SON, N., KANG,
676 G., KIM, J., KIM, K., PARK, M. S., KIM, Y. K. & BAEK, D. 2021a. A high-resolution temporal atlas of
677 the SARS-CoV-2 translatome and transcriptome. *Nat Commun,* 12**,** 5120.

678 KIM, D., SUNG, Y. M., PARK, J., KIM, S., KIM, J., PARK, J., HA, H., BAE, J. Y., KIM, S. & BAEK, D.
679 2016. General rules for functional microRNA targeting. *Nat Genet,* 48**,** 1517-1526.

680 KIM, J. H., PARK, I., SHIN, H. R., RHEE, J., SEO, J. Y., JO, Y. W., YOO, K., HANN, S. H., KANG, J.
681 S., PARK, J., KIM, Y. L., MOON, J. Y., CHOI, M. H. & KONG, Y. Y. 2021b. The hypothalamic-pituitary-
682 gonadal axis controls muscle stem cell senescence through autophagosome clearance. *J Cachexia*
683 *Sarcopenia Muscle,* 12**,** 177-191.

KOLBERG, L., RAUDVERE, U., KUZMIN, I., ADLER, P., VILO, J. & PETERSON, H. 2023. g:Profiler-interoperable web service for functional enrichment analysis and gene identifier mapping (2023 update). *Nucleic Acids Res,* 51**,** W207-W212.

LANGMEAD, B. & SALZBERG, S. L. 2012. Fast gapped-read alignment with Bowtie 2. *Nat Methods,* 9**,** 357-9.

LIU, L., CHARVILLE, G. W., CHEUNG, T. H., YOO, B., SANTOS, P. J., SCHROEDER, M. & RANDO, T. A. 2018. Impaired Notch Signaling Leads to a Decrease in p53 Activity and Mitotic Catastrophe in Aged Muscle Stem Cells. *Cell Stem Cell,* 23**,** 544-556 e4.

LIU, L., CHEUNG, T. H., CHARVILLE, G. W., HURGO, B. M., LEAVITT, T., SHIH, J., BRUNET, A. & RANDO, T. A. 2013. Chromatin modifications as determinants of muscle stem cell quiescence and chronological aging. *Cell Rep,* 4**,** 189-204.

LIU, L., CHEUNG, T. H., CHARVILLE, G. W. & RANDO, T. A. 2015. Isolation of skeletal muscle stem cells by fluorescence-activated cell sorting. *Nat Protoc,* 10**,** 1612-24.

LOVE, M. I., HUBER, W. & ANDERS, S. 2014. Moderated estimation of fold change and dispersion for RNA-seq data with DESeq2. *Genome Biol,* 15**,** 550.

MARTIN, M. 2011. Cutadapt removes adapter sequences from high-throughput sequencing reads. *2011,* 17**,** 3.

MAURO, A. 1961. Satellite cell of skeletal muscle fibers. *J Biophys Biochem Cytol,* 9**,** 493-5.

NAGY, E. & MAQUAT, L. E. 1998. A rule for termination-codon position within intron-containing genes: when nonsense affects RNA abundance. *Trends Biochem Sci,* 23**,** 198-9.

OPRESCU, S. N., YUE, F., QIU, J., BRITO, L. F. & KUANG, S. 2020. Temporal Dynamics and Heterogeneity of Cell Populations during Skeletal Muscle Regeneration. *iScience,* 23**,** 100993.

PALA, F., DI GIROLAMO, D., MELLA, S., YENNEK, S., CHATRE, L., RICCHETTI, M. & TAJBAKHSH, S. 2018. Distinct metabolic states govern skeletal muscle stem cell fates during prenatal and postnatal myogenesis. *J Cell Sci,* 131.

PRICE, F. D., VON MALTZAHN, J., BENTZINGER, C. F., DUMONT, N. A., YIN, H., CHANG, N. C., WILSON, D. H., FRENETTE, J. & RUDNICKI, M. A. 2014. Inhibition of JAK-STAT signaling stimulates adult satellite cell function. *Nat Med,* 20**,** 1174-81.

PRUITT, K. D., TATUSOVA, T. & MAGLOTT, D. R. 2007. NCBI reference sequences (RefSeq): a curated non-redundant sequence database of genomes, transcripts and proteins. *Nucleic Acids Res,* 35**,** D61-5.

RISSO, D., NGAI, J., SPEED, T. P. & DUDOIT, S. 2014. Normalization of RNA-seq data using factor analysis of control genes or samples. *Nat Biotechnol,* 32**,** 896-902.

RYGIEL, K., PICARD, M. & TURNBULL, D. 2016. The ageing neuromuscular system and sarcopenia: a mitochondrial perspective. *J Physiol,* 594**,** 4499--4512.

SACCO, A., DOYONNAS, R., KRAFT, P., VITOROVIC, S. & BLAU, H. M. 2008. Self-renewal and expansion of single transplanted muscle stem cells. *Nature,* 456**,** 502-6.

SAITO, Y. & CHIKENJI, T. S. 2021. Diverse Roles of Cellular Senescence in Skeletal Muscle Inflammation, Regeneration, and Therapeutics. *Front Pharmacol,* 12**,** 739510.

SANTOS, M. D., GIOFTSIDI, S., BACKER, S., MACHADO, L., RELAIX, F., MAIRE, P. & MOURIKIS, P. 2021. Extraction and sequencing of single nuclei from murine skeletal muscles. *STAR Protocols,* 2.

SCHULER, S. C., KIRKPATRICK, J. M., SCHMIDT, M., SANTINHA, D., KOCH, P., DI SANZO, S., CIRRI, E., HEMBERG, M., ORI, A. & VON MALTZAHN, J. 2021. Extensive remodeling of the extracellular matrix during aging contributes to age-dependent impairments of muscle stem cell functionality. *Cell Rep,* 35**,** 109223.

SEALE, P., SABOURIN, L. A., GIRGIS-GABARDO, A., MANSOURI, A., GRUSS, P. & RUDNICKI, M. A. 2000. Pax7 is Required for the Specification of Myogenic Satellite cells. *Cell,* 102**,** 777-786.

TANG, H., INOKI, K., BROOKS, S. V., OKAZAWA, H., LEE, M., WANG, J., KIM, M., KENNEDY, C. L., MACPHERSON, P. C. D., JI, X., VAN ROEKEL, S., FRAGA, D. A., WANG, K., ZHU, J., WANG, Y., SHARP, Z. D., MILLER, R. A., RANDO, T. A., GOLDMAN, D., GUAN, K. L. & SHRAGER, J. B. 2019. mTORC1 underlies age-related muscle fiber damage and loss by inducing oxidative stress and catabolism. *Aging Cell,* 18**,** e12943.

WASKOM, M. L. 2021. seaborn: statistical data visualization. *JOSS,* 6**,** 3021.

XU, M., PIRTSKHALAVA, T., FARR, J. N., WEIGAND, B. M., PALMER, A. K., WEIVODA, M. M., INMAN, C. L., OGRODNIK, M. B., HACHFELD, C. M., FRASER, D. G., ONKEN, J. L., JOHNSON, K. O., VERZOSA, G. C., LANGHI, L. G. P., WEIGL, M., GIORGADZE, N., LEBRASSEUR, N. K., MILLER, J. D., JURK, D., SINGH, R. J., ALLISON, D. B., EJIMA, K., HUBBARD, G. B., IKENO, Y., CUBRO, H., GAROVIC, V. D., HOU, X., WEROHA, S. J., ROBBINS, P. D., NIEDERNHOFER, L. J., KHOSLA, S., TCHKONIA, T. & KIRKLAND, J. L. 2018. Senolytics improve physical function and increase lifespan in old age. *Nat Med,* 24**,** 1246-1256.

ZHANG, H., RYU, D., WU, Y., GARIANI, K., WANG, X., LUAN, P., D'AMICO, D., ROPELLE, E. R., LUTOLF, M. P., AEBERSOLD, R., SCHOONJANS, K., MENZIES, K. J. & AUWERX, J. 2016. NAD(+) repletion improves mitochondrial and stem cell function and enhances life span in mice. *Science,* 352**,** 1436-43.

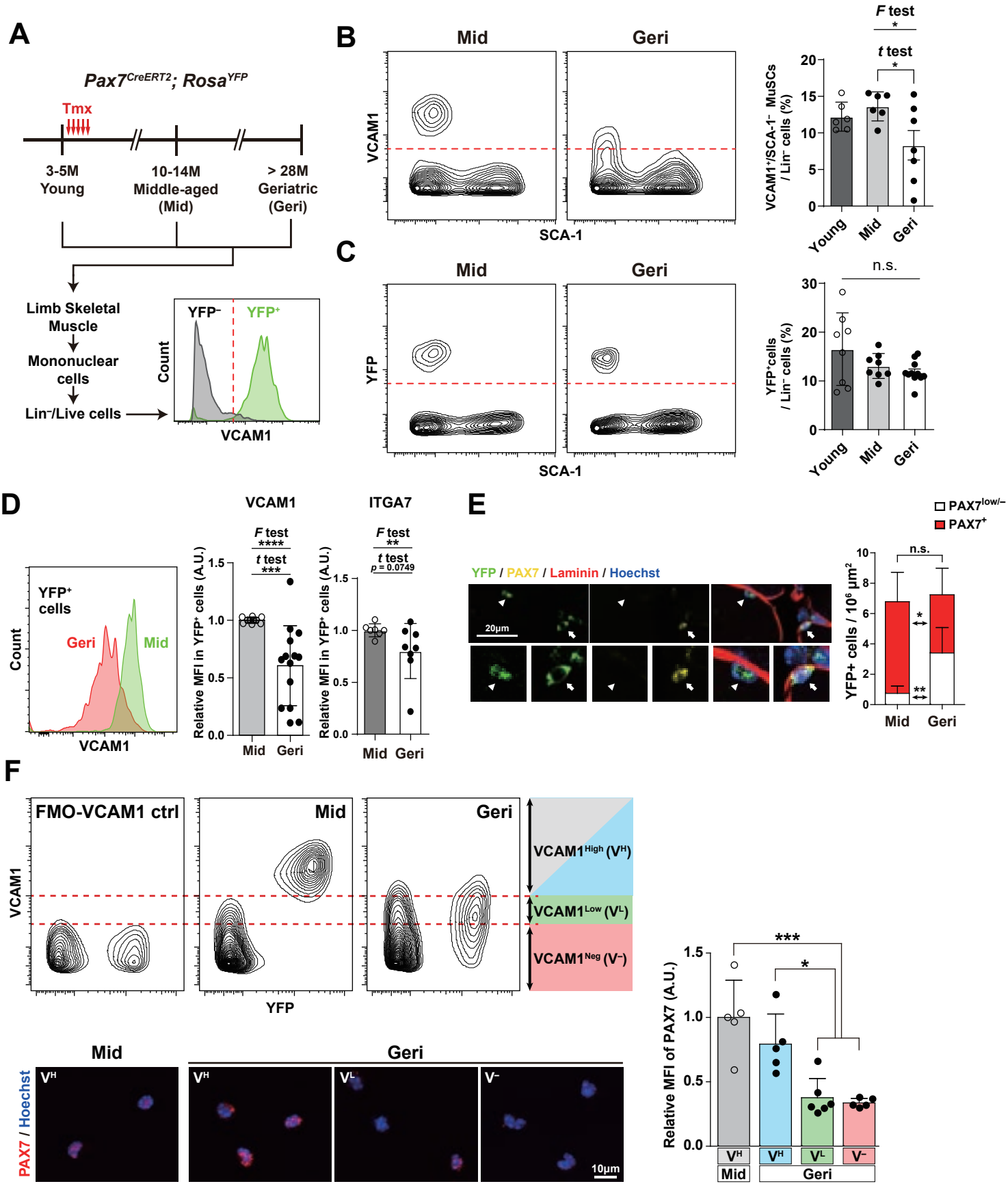
A
Pax7CreERT2; RosaYFP
Tmx
3-5M Young
10-14M Middle-aged (Mid)
> 28M Geriatric (Geri)
Limb Skeletal Muscle
Mononuclear cells
Lin−/Live cells
YFP−
YFP+
Count
VCAM1
B
Mid
Geri
VCAM1
SCA-1
F test
t test
VCAM1+/SCA-1− MuSCs / Lin− cells (%)
Young
Mid
Geri
C
YFP
n.s.
YFP+cells / Lin− cells (%)
D
VCAM1
ITGA7
YFP+ cells
Relative MFI in YFP+ cells (A.U.)
p = 0.0749
E
PAX7low/−
PAX7+
YFP / PAX7 / Laminin / Hoechst
20μm
YFP+ cells / 10^6 μm^2
F
FMO-VCAM1 ctrl
VCAM1High (VH)
VCAM1Low (VL)
VCAM1Neg (V−)
PAX7 / Hoechst
10μm
Relative MFI of PAX7 (A.U.)

749 **Figure. 1. The YFP$^+$ cells from *Pax7^{CreERT2};Rosa^{YFP}* mice do not decrease with age.** (**A**)
750 Scheme of MuSC labeling in *Pax7^{CreERT2};Rosa^{YFP}* mice (MuSC^{YFP}) and analysis at middle (Mid)
751 and geriatric age (Geri) using fluorescence-activated cell sorting (FACS) strategy for isolation of
752 YFP$^+$ MuSCs using traditional marker, VCAM1. (**B, C**) Representative plot and quantification for
753 VCAM1$^+$ MuSCs (**B**) and YFP$^+$ cells (**C**) in lineage negative (Lin$^-$) cells of Young (n=6 and n=8
754 each), Mid (n = 7, n = 8, each) and Geri (n = 6, n = 11, each) MuSC^{YFP}, Welch's *t* test and *F*-test;
755 p = 0.0441 and 0.0460 for (**B**), respectively. (**D**) Representative FACS histogram and
756 quantification of VCAM1 and ITGA7 expression in YFP$^+$ cells of Mid and Geri MuSC^{YFP}.
757 Quantification of relative VCAM1 and ITGA7 mean fluorescence intensity (MFI) in YFP$^+$ cells
758 of Mid (n = 12, n = 6, each) and Geri (n = 14, n = 8, each) MuSC^{YFP}, Welch's *t* test and *F*-test; p
759 = 0.0009 and <0.0001. (**E**) Representative images and quantification of immunohistochemistry
760 staining for Hoechst (Blue), YFP (Green), PAX7 (Yellow), and Laminin (Red) in the *Tibialis*
761 *Anterior* (TA) of MuSC^{YFP}. Arrows indicate PAX7$^+$/YFP$^+$ cells and arrowheads indicate PAX7$^-$
762 /YFP$^+$ cells under basal lamina. Quantification of the number of Pax7$^+$/YFP$^+$ and PAX7$^-$/YFP$^+$
763 cells from IHC staining of TA in Mid (n = 7) and Geri (n = 9) MuSC^{YFP}, two-way ANOVA
764 followed by Bonferroni's multiple comparison test, PAX7$^+$/YFP$^+$; p = 0.0205, PAX7$^-$/YFP$^+$; p =
765 0.0051. (**F**) Division of YFP$^+$ cells according to their VCAM1 MFI as VCAM1^{High} (V^H),
766 VCAM1^{Low} (V^L), and VCAM1^{Neg} (V$^-$) followed by representative images and quantification of
767 immunocytochemistry (ICC) staining for Hoechst (Blue), PAX7 (Red) of YFP$^+$ cells. VCAM1
768 low and negative MuSCs represent approximately 44.6% ± 35.7%, whereas VCAM1 high MuSCs
769 represent 3.9% ± 1.8%. Quantification of PAX7 fluorescence intensity from isolated YFP$^+$ cells
770 of Mid V^H, Geri V^H, V$^-$ (n = 5, each), and V^L (n=6), one-way ANOVA followed by Bonferroni's

771 multiple comparison test; p = 0.0004 (vs Mid V^H), and 0.0179, 0.0123 (Geri V^H vs V^L, V^-,

772 respectively).

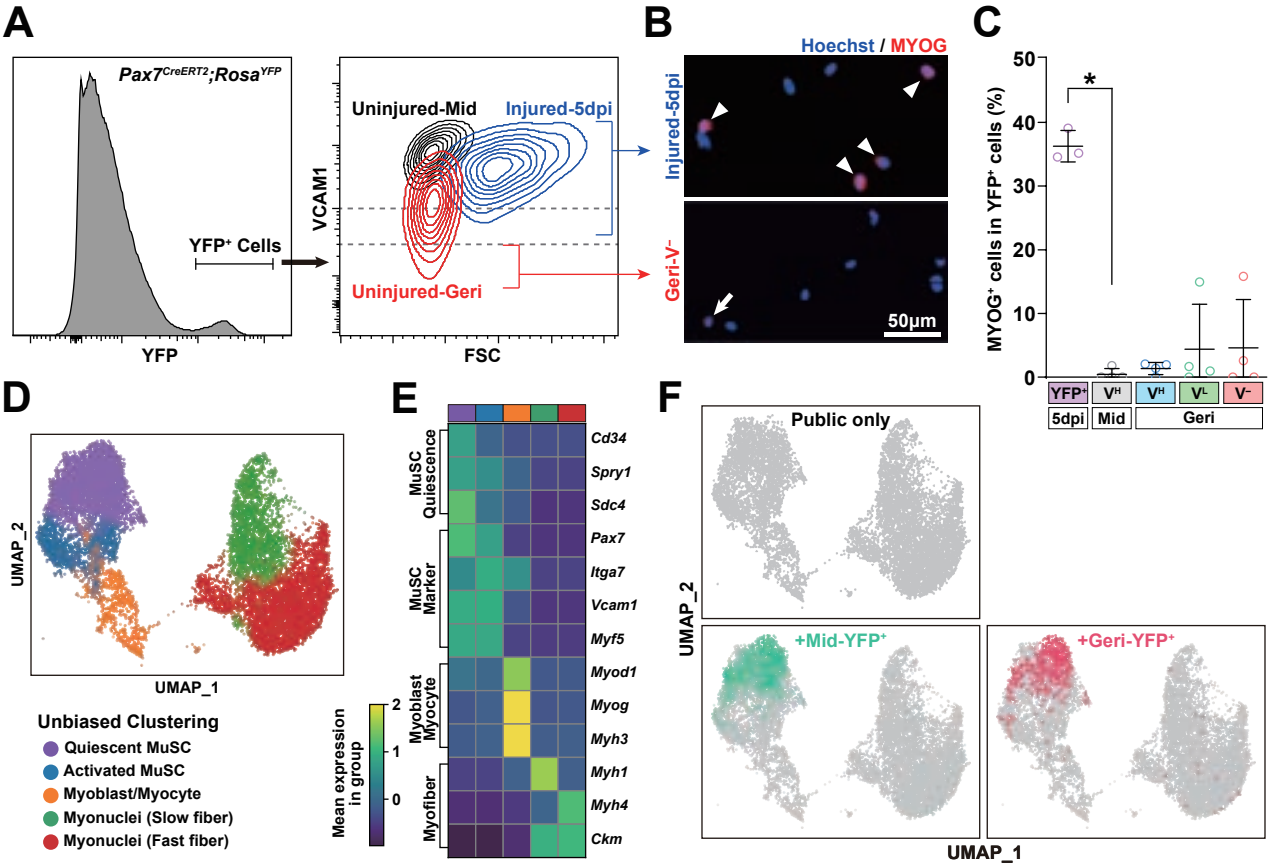
A
Pax7CreERT2;RosaYFP
YFP+ Cells
YFP
VCAM1
FSC
Uninjured-Mid
Injured-5dpi
Uninjured-Geri
B
Hoechst / MYOG
Injured-5dpi
Geri-V-
50µm
C
MYOG+ cells in YFP+ cells (%)
50
40
30
20
10
0
*
YFP+
VH
VH
VL
V-
5dpi
Mid
Geri
D
UMAP_2
UMAP_1
Unbiased Clustering
Quiescent MuSC
Activated MuSC
Myoblast/Myocyte
Myonuclei (Slow fiber)
Myonuclei (Fast fiber)
E
MuSC Quiescence
MuSC Marker
Myoblast Myocyte
Myofiber
Cd34
Spry1
Sdc4
Pax7
Itga7
Vcam1
Myf5
Myod1
Myog
Myh3
Myh1
Myh4
Ckm
Mean expression in group
2
1
0
F
Public only
+Mid-YFP+
+Geri-YFP+
UMAP_2
UMAP_1

773 **Figure 2. YFP$^+$/VCAM1$^-$ cells are quiescent MuSCs.** (**A**) Representative FACS plot for YFP$^+$
774 cells from uninjured Mid and Geri, and injured-5dpi young (20-weeks-old) mice. (**B**, **C**)
775 Representative images (**B**) of ICC staining for Hoechst (Blue) and MYOG (Red), and
776 quantification (**C**) of MYOG$^+$ cells in each YFP$^+$ cell, one-way ANOVA followed by Bonferroni's
777 multiple comparison test; p = 0.0139 between YFP+ cells of injured-5dpi and Mid V^H. While 5
778 dpi MuSCs differed significantly from young MuSCs (adjusted p = 0.0139), the comparisons
779 between 5 dpi and each geriatric subgroup (VCAM-high, -mid, and -low) did not reach statistical
780 significance after correction for multiple testing (adjusted p = 0.17, 0.15, and 0.17, respectively).
781 (**D**) Uniform manifold approximation and projection (UMAP) plot of YFP$^+$ cells integrated with
782 public scRNA-seq data of MuSC-lineage mononucleated cells in uninjured/injured muscle colored
783 by cell types. (**E**) Matrix plot for representative genes of specific cell types for determining the
784 identities of each cluster. (**F**) The localization of Mid and Geri YFP$^+$ cells in this study on UMAP
785 plot of Fig. 2D.

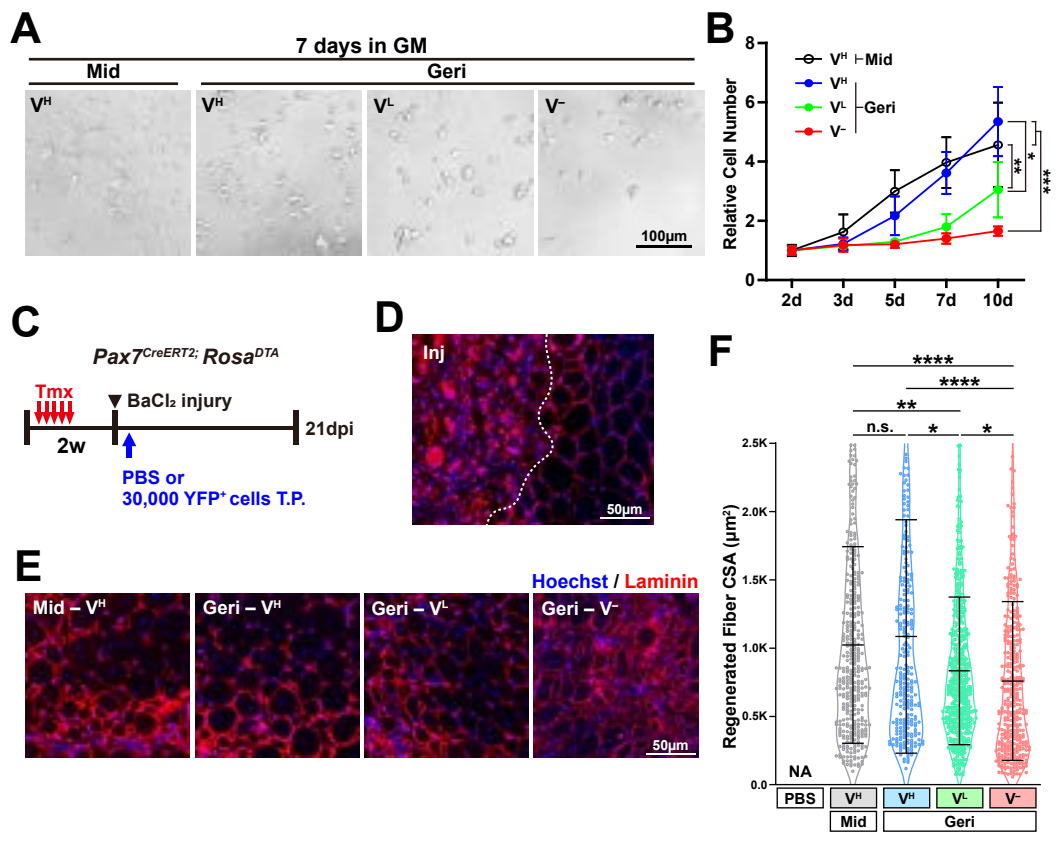
A
7 days in GM
Mid
Geri
V^H
V^H
V^L
V^-
100μm
B
Relative Cell Number
V^H Mid
V^H
V^L
V^- Geri
2d
3d
5d
7d
10d
C
Pax7^CreERT2; Rosa^DTA
Tmx
BaCl₂ injury
2w
21dpi
PBS or
30,000 YFP⁺ cells T.P.
D
Inj
50μm
E
Hoechst / Laminin
Mid – V^H
Geri – V^H
Geri – V^L
Geri – V^-
50μm
F
Regenerated Fiber CSA (μm²)
n.s.
NA
PBS
V^H
V^H
V^L
V^-
Mid
Geri

786 **Figure 3. Compromised but retained functionality in VCAM1^{-} MuSCs.** (**A**) Representative
787 bright field images of Mid V^H, Geri V^H, V^L, and V^- MuSCs at 7 days culture in MuSC growth
788 media. (**B**) Proliferation measured by relative cell number at 2, 3, 5, 7, and 10 days, two-way
789 ANOVA followed by Bonferroni's multiple comparison test; p = 0.0029 and 0.0002 (Mid V^H vs
790 V^L and V^-, respectively) and p= 0.0102 and 0.0006 (Geri V^H vs VL and V^-, respectively). For each
791 sample, 30,000 MuSCs were plated at day 0, with 3 biological replicates per condition. (**C**)
792 Experimental schematics of transplantation of YFP$^+$ cells to TA muscle of *Pax7^{CreERT2};Rosa^{DTA}*
793 mice. (**D, E**) Representative images of IHC staining for Hoechst (Blue) and Laminin (Red) in PBS
794 treated TA muscle section following injury. (**D**) Left side of the dotted line show areas affected by
795 BaCl2 injury and right side shows uninjured areas of the muscle. (**E**) IHC staining shows
796 centralized myofibers in all images, with notably smaller myofibers in Geri V^-. (**F**) Quantification
797 of cross-sectional area (CSA) of regenerated fibers from TA muscle of *Pax7^{CreERT2};Rosa^{DTA}* mice
798 transplanted with Mid V^H, Geri V^H, V^L, and V^- at 21 dpi, n = 3 for each group. For each mouse,
799 the entire TA muscle was cryosectioned and immunostained, and all regenerated fibers containing
800 centrally located nuclei were included in the CSA quantification. Total 43 data points are outside
801 of the axis. Kruskal-Wallis test followed by Dunn's multiple comparison test; $p < 0.0001$ (Mid and
802 Geri V^H vs V^-) and p = 0.0059 (Mid V^H vs Geri V^L), 0.0149 (Geri V^H vs V^L) and 0.0143 (Geri V^L
803 vs V^-).

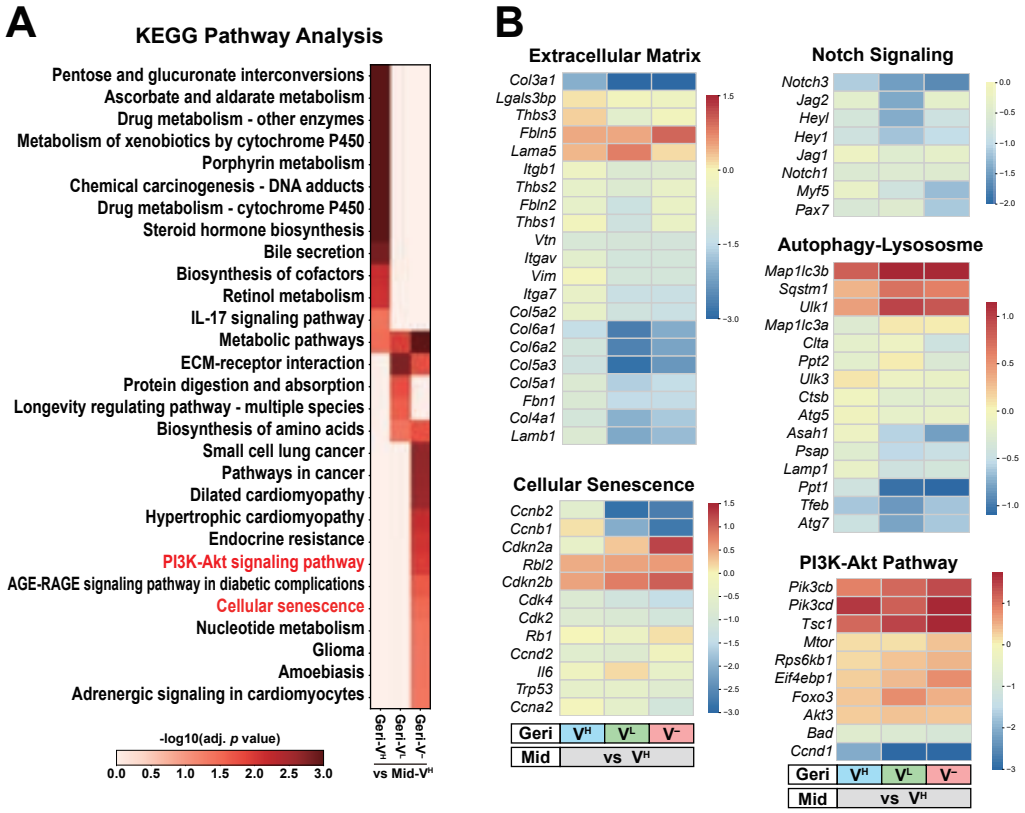
A
KEGG Pathway Analysis
Pentose and glucuronate interconversions
Ascorbate and aldarate metabolism
Drug metabolism - other enzymes
Metabolism of xenobiotics by cytochrome P450
Porphyrin metabolism
Chemical carcinogenesis - DNA adducts
Drug metabolism - cytochrome P450
Steroid hormone biosynthesis
Bile secretion
Biosynthesis of cofactors
Retinol metabolism
IL-17 signaling pathway
Metabolic pathways
ECM-receptor interaction
Protein digestion and absorption
Longevity regulating pathway - multiple species
Biosynthesis of amino acids
Small cell lung cancer
Pathways in cancer
Dilated cardiomyopathy
Hypertrophic cardiomyopathy
Endocrine resistance
PI3K-Akt signaling pathway
AGE-RAGE signaling pathway in diabetic complications
Cellular senescence
Nucleotide metabolism
Glioma
Amoebiasis
Adrenergic signaling in cardiomyocytes
-log10(adj. p value)
0.0 0.5 1.0 1.5 2.0 2.5 3.0
Geri-VH
Geri-VL
Geri-V-
vs Mid-VH
B
Extracellular Matrix
Col3a1
Lgals3bp
Thbs3
Fbln5
Lama5
Itgb1
Thbs2
Fbln2
Thbs1
Vtn
Itgav
Vim
Itga7
Col5a2
Col6a1
Col6a2
Col5a3
Col5a1
Fbn1
Col4a1
Lamb1
Notch Signaling
Notch3
Jag2
Heyl
Hey1
Jag1
Notch1
Myf5
Pax7
Autophagy-Lysosome
Map1lc3b
Sqstm1
Ulk1
Map1lc3a
Clta
Ppt2
Ulk3
Ctsb
Atg5
Asah1
Psap
Lamp1
Ppt1
Tfeb
Atg7
Cellular Senescence
Ccnb2
Ccnb1
Cdkn2a
Rbl2
Cdkn2b
Cdk4
Cdk2
Rb1
Ccnd2
Il6
Trp53
Ccna2
PI3K-Akt Pathway
Pik3cb
Pik3cd
Tsc1
Mtor
Rps6kb1
Eif4ebp1
Foxo3
Akt3
Bad
Ccnd1
Geri VH VL V-
Mid vs VH

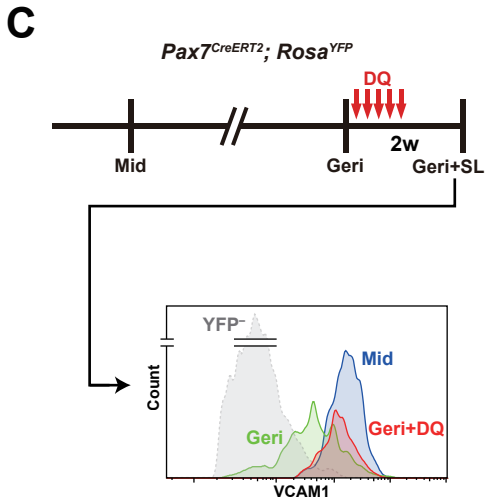
C
Pax7CreERT2; RosaYFP
DQ
Mid
Geri
2w
Geri+SL
YFP-
Mid
Geri
Geri+DQ
Count
VCAM1

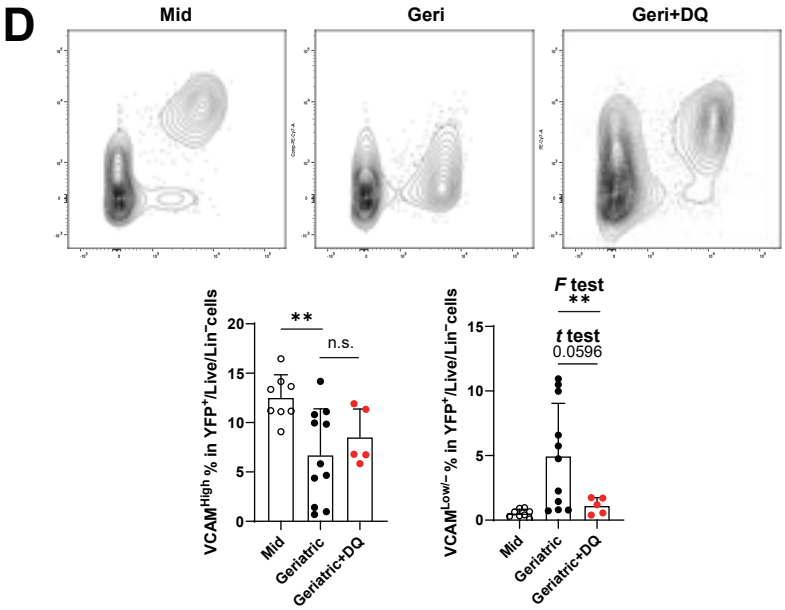
D
Mid
Geri
Geri+DQ
VCAMHigh % in YFP+/Live/Lin-cells
**
n.s.
Mid
Geriatric
Geriatric+DQ
VCAMLow/- % in YFP+/Live/Lin-cells
F test
**
t test
0.0596

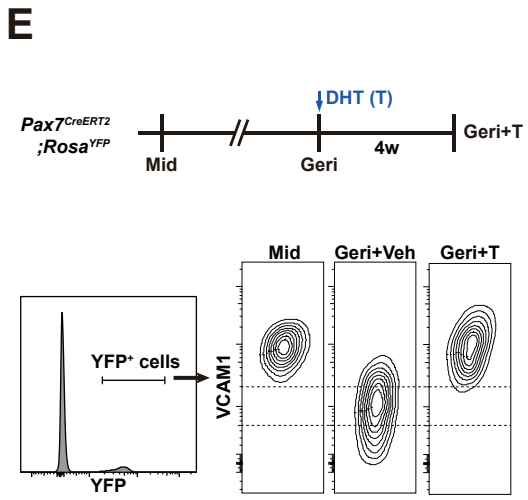
E
Pax7CreERT2 ;RosaYFP
DHT (T)
Mid
Geri
4w
Geri+T
YFP+ cells
YFP
VCAM1
Mid
Geri+Veh
Geri+T

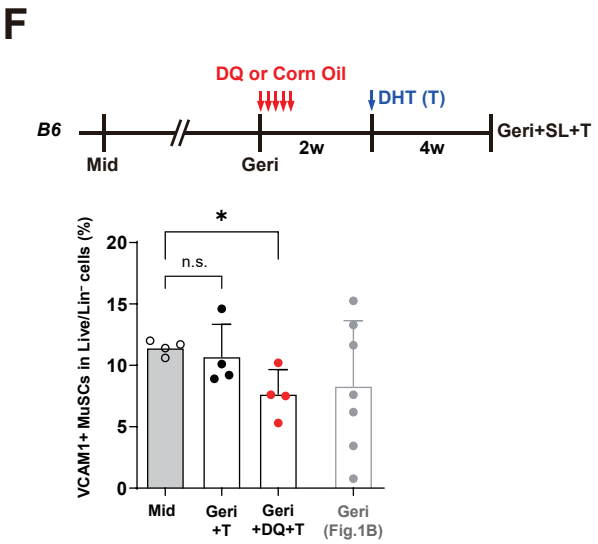
F
DQ or Corn Oil
B6
DHT (T)
Mid
Geri
2w
4w
Geri+SL+T
VCAM1+ MuSCs in Live/Lin- cells (%)
*
n.s.
Mid
Geri +T
Geri +DQ+T
Geri (Fig.1B)

804 **Figure 4. Senescence characteristics of VCAM1^{-}/YFP^{+} cells and their rejuvenation by DHT**
805 **supplementation.** (**A**) The statistical significance of Kyoto-Encyclopedia of Genes and Genomes
806 (KEGG) pathways, associated with differentially expressed genes (DEGs) between Mid V^{H} and
807 Geri V^{H}, V^{L} and V^{-}, visualized as a heatmap. (**B**) Heatmap of relative expressions of representative
808 genes known to be altered in aged MuSCs compared to Mid V^{H}. (**C**) Experimental schematics of
809 senolytics, dasatinib and quercetin (DQ), treatment in MuSC^{YFP} at geriatric age and representative
810 FACS histogram of VCAM1 expression Mid, Geri, and Geri treated with SL (Geri+DQ) mice. (**D**)
811 Representative FACS plots and quantification of the percentage of VCAM1^{High} and VCAM1$^{Low/-}$
812 cells divided by VCAM1 expression levels in Mid (n = 8) and Geri mice with (n = 5) or without
813 (n = 11) senolytics, 2 tailed student's t test, p = 0.0051 for Mid vs Geri in VCAM1^{High} and F test:
814 p = 0.0026 for Geriatric vs Geriatric+DQ in VCAM1$^{Low/-}$. (**E**) Experimental schematics of
815 dihydrotestosterone (DHT) treatment and FACS plot of VCAM1 expression levels for YFP^{+} cells
816 in MuSC^{YFP}. (**F**) Experimental schematics of DQ and DHT treatment and quantification of the
817 percentage of VCAM1^{High} MuSCs in Live/Lin– cells in Mid and Geri B6 mice (n = 4 in each), 2
818 tailed student's t test, p = 0.0113 for Young vs Geri+DQ+T.

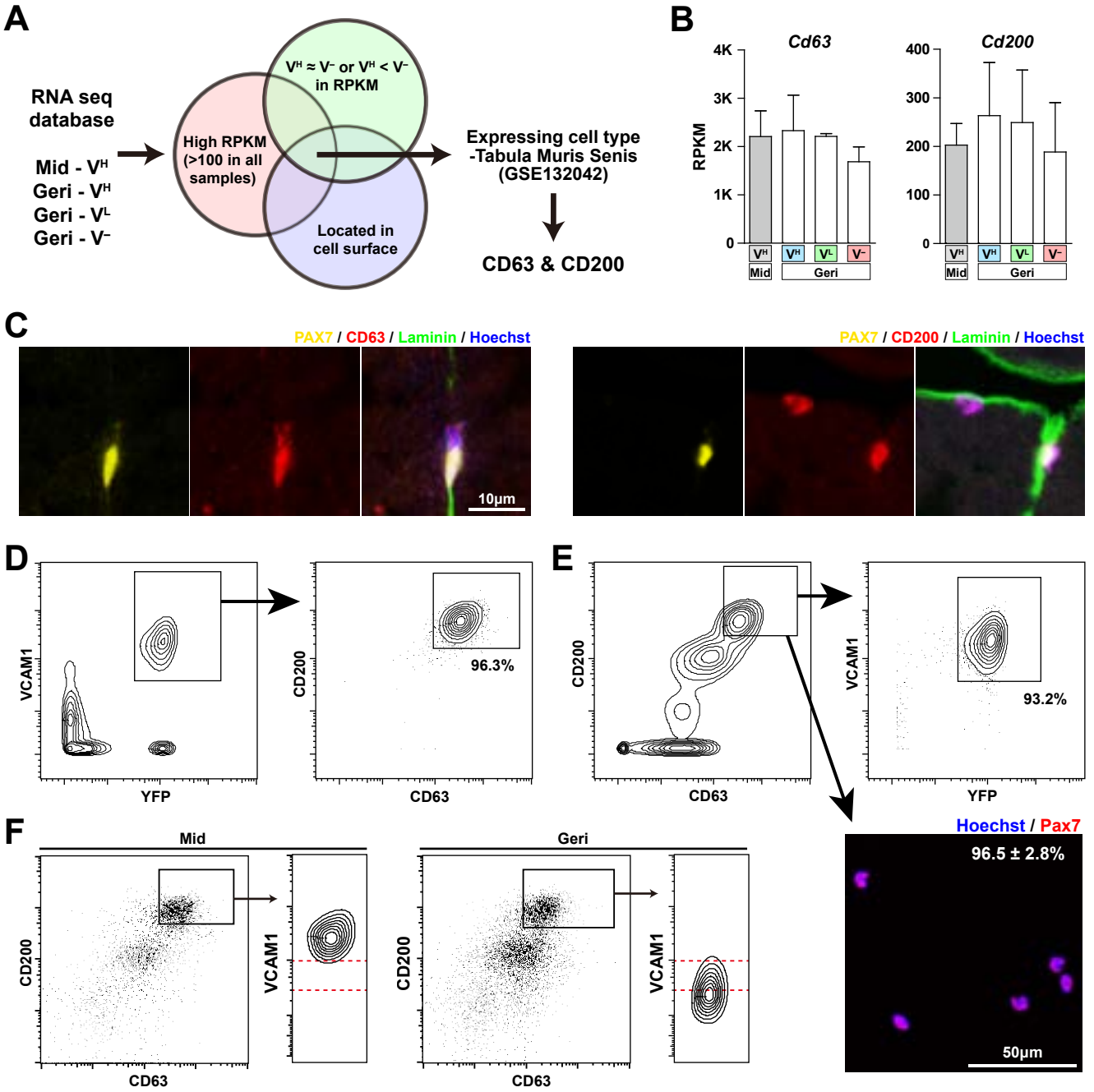
A
RNA seq database
Mid - V^H
Geri - V^H
Geri - V^L
Geri - V^-
High RPKM (>100 in all samples)
V^H ≈ V^- or V^H < V^- in RPKM
Located in cell surface
Expressing cell type -Tabula Muris Senis (GSE132042)
CD63 & CD200
B
Cd63
Cd200
RPKM
4K
3K
2K
1K
0
400
300
200
100
0
V^H
V^H
V^L
V^-
Mid
Geri
C
PAX7 / CD63 / Laminin / Hoechst
10μm
PAX7 / CD200 / Laminin / Hoechst
D
VCAM1
YFP
CD200
CD63
96.3%
E
CD200
CD63
VCAM1
YFP
93.2%
F
Mid
Geri
CD200
CD63
VCAM1
Hoechst / Pax7
96.5 ± 2.8%
50μm

819 **Figure 5. Detection of GERI-MuSCs using CD63/CD200-based FACS strategy.** (**A**) Vann
820 Diagram schematics showing criteria used to select MuSC marker candidate CD63 and CD200,
821 from RNA seq database. (**B**) Relative gene expressions of *Cd63* and *Cd200* shown in RPKMs from
822 Mid V^H, Geri V^H, V^L, and V^- MuSCs. (**C**, **D**) Representative IHC staining images for Hoechst
823 (Blue), Laminin (Green), PAX7 (Yellow) with CD63 (red, **C**) or CD200 (red, **D**) in the TA muscle
824 of Mid $MuSC^{YFP}$. (**E**) Representative FACS plot from young mice showing 96.3% of
825 $VCAM1^+/YFP^+$ cells are $CD63^{high}/CD200^{high}$. (**F**) Left: representative FACS plot from young mice
826 showing 93.2% of $CD63^{high}/CD200^{high}$ cells are $VCAM1^+/YFP^+$, and ICC staining of this
827 population shows that 96.5±2.8% are $PAX7^+$. Right: representative FACS plot of MuSCs of *B6*
828 Mid and Geri mice gated by CD63 and CD200 and their VCAM1 expression level.